Computing the Noise Temperature Increase Caused by Pointing DSS 13 at the Center of the Moon

W. A. Imbriale[1]

The Moon radiates energy at microwave wavelengths and, as a result, an antenna pointed at or near the Moon will experience an increase in receiver noise temperature that needs to be accounted for in telecommunications link calculations or in any radio science or ranging activities. This article computes the noise-temperature increases caused by pointing the Deep Space Station 13 (DSS 13) beam-waveguide antenna at the center of the Moon at 2.295-GHz (S-band), 8.45-GHz (X-band), and 32-GHz (Ka-band) frequencies and compares them to the measured values.

I. Introduction

The Moon radiates energy at infrared and microwave wavelengths, in addition to the reflecting of sunlight at visible wavelengths. When one views the Moon, one perceives the light reflected from the Sun. This is manifested in the synodic lunar phase cycle that repeats as the Moon orbits the Earth. The period of lunation or repetition of lunar phases occurs at a synodic period of about 29.5 days, a lunar month. At other wavelengths, there is very little reflected radiation, so the emission is dominated by thermal emission that is related to the Moon's surface temperature, which in turn is related to the properties of the lunar surface material and the amount of sunlight incident upon it. For the Moon, the infrared emission variation is well correlated with lunar phase cycle as it originates from a thin surface layer of the Moon.

However, at millimeter and centimeter radio wavelengths, the degree of this variation is much less than at infrared due to the fact that radio emission originates from some depth below the surface. The surface layers are heated by conduction, and thus the variations in the radio lag behind the lunar phase cycle of solar heating. Hence, the longer the wavelength, the deeper the surface from which the radiation is emitted. The amplitude and phase of the variation are wavelength dependent, and the phase is consistent with that of the solar insolation. The degree of variation versus lunar phase observed for radio wavelengths longer than 5 cm is not significant.

With the prospect of revisiting the Moon with future human and robotic expeditions, the realization of very high data rates requires a thorough understanding of all contributions in the link calculations.

---

[1] Communications Ground Systems Section.

The research described in this publication was carried out by the Jet Propulsion Laboratory, California Institute of Technology, under a contract with the National Aeronautics and Space Administration.

Among these contributions, the additional system noise-temperature increase while pointing a large-diameter antenna onto the disk of the moon must be characterized, either by modeling or by direct measurement. Morabito [1] conducted a series of measurements on the NASA Deep Space Network 34-m beam-waveguide (BWG) antennas to measure these temperature increases. This information is needed for communication links at different frequencies—2.295 GHz (S-band), 8.45 GHz (X-band), and 32 GHz (Ka-band). This article will provide an analytical model for computing this temperature increase and compare it to Morabito's measured results.

To assist in this calculation, brightness-temperature maps of the Moon were made available by Steve Keihm at S-band, X-band, and Ka-band. These maps consist of two-dimensional arrays of Earth-viewed brightness temperatures of the lunar surface for lunar phase angles from 0 to 360 deg in steps of 12 deg. These are theoretical pencil-beam maps that were generated based on properties of the lunar soil derived from Apollo program findings, and have been validated from Earth-based measurements made in the 1960s from 1 mm to 10 cm.

Using Keihm's maps and the computed radiation patterns of the Deep Space Station 13 (DSS 13) antenna, the noise-temperature increase caused by pointing the antenna at the Moon can be determined. The following describes the methodology used.

II. Analysis Technique

A familiar expression for antenna noise temperature in the spherical coordinate system is

$$T_A = \frac{\int_0^{\pi}\int_0^{2\pi} P(\theta,\phi)T_b(\theta,\phi)\sin\theta d\phi d\theta}{\int_0^{\pi}\int_0^{2\pi} P(\theta,\phi)\sin\theta d\phi d\theta} \tag{1}$$

where

$P(\theta,\phi) =$ power per unit solid angle in any direction (θ,ϕ)

$T_b(\theta,\phi) =$ brightness temperature, K

Since the denominator of Eq. (1) is the total radiated power, P_T, and the antenna gain, $G(\theta,\phi)$, in any direction is [1]

$$G(\theta,\phi) = 4\pi\frac{P(\theta,\phi)}{P_T} \tag{2}$$

substitution into Eq. (1) gives another familiar expression of

$$T_A = \frac{1}{4\pi}\int_0^{\pi}\int_0^{2\pi} G(\theta,\phi)T_b(\theta,\phi)\sin\theta d\phi d\theta \tag{3}$$

To compute the noise temperature increase caused by the Moon, it is necessary to integrate the brightness temperature of the Moon plus the background and subtract it from the integration of the brightness temperature of the background. This yields the expression for the noise temperature as

$$T_D = \frac{1}{4\pi}\iint_{\text{Moon}} G(\theta,\phi)T_M(\theta,\phi)\sin\theta d\theta d\phi \tag{4}$$

where the integration is over only the Moon. It is now necessary to determine $G(\theta, \phi)$ for the DSS 13 antenna at the frequencies of interest.

The geometry of the BWG antenna is described in [2]. The two configurations to be analyzed are the S- and X-band frequencies for the S-/X-band feed position and the X- and Ka-band frequencies for the X-/Ka-band position. The geometry for the S-/X-band position is shown in Fig. 1. The configuration is analyzed for the transmit mode, and reciprocity is used for the received mode. Initially the pattern for the corrugated horn is computed using the horn geometry and mode-matching software described in [2, Chapter 1]. The horn pattern then is used to determine the physical optics (PO) currents on the first mirror. The currents on the first mirror then are used to determine the currents on the second mirror, as also described in [2, Chapter 1]. Note that proper power normalization is utilized as all the power from the feed does not get to the second mirror, but some is spilled past the first mirror. The procedure then is repeated for each of the mirrors, the subreflector, and the main reflector. The currents radiating from the main reflector then are utilized to obtain $G(\theta, \phi)$. For accuracy and completeness, the actual distorted shape of the main reflector (the distortion is sufficient to affect the pattern at X- and Ka-bands) and the subreflector and strut blocking pattern are required. The latter two effects were determined from holography measurements on the DSS 13 antenna as described in [3].

For blockage considerations, consider the pattern shown in Fig. 2 as measured from holography. The blockage mask then applied to the main reflector current distribution (the PO currents set to zero) is shown in Fig. 3.

III. S-Band Results

Using the geometry from Fig. 1(b) and the strut mask of Fig. 3, the far-field radiation pattern was computed at 2.3 GHz and is shown in Fig. 4. Substituting this pattern in Eq. (4) and using one of Keihm's S-band maps, a noise temperature of 136 K is computed. Applying an atmosphere correction of 1.017 gives a temperature of 134 K. Since there is little variation with Moon phase, this number is compared to the measured values in Fig. 5.

IV. X-Band Results

Measurements were made at X-band for both the S-/X-band position and the X-/Ka-band position. However, from a theoretical design consideration, both designs are identical. Using the geometry shown in Fig. 1(b), the strut mask of Fig. 3, and the measured panel distortion at the rigging angle derived from [3], the far-field radiation pattern was computed and is shown in Fig. 6. The pattern then was convolved with the Keihm maps for the various Moon phases, an atmospheric correction of 1.02 was applied, and the results were plotted in Fig. 7 in comparison to the measured values.

V. Ka-Band Results

Measurements were made at Ka-band at the X-/Ka-band position shown in Fig. 8. Using the geometry shown in Fig. 8, the strut mask of Fig. 3, and the measured main reflector distortion at the rigging angle, the far-field radiation pattern was computed at 32 GHz and is shown in Fig. 9. To compare this to the measured values, an additional factor needs to be applied to the calculated pattern, and that is the loss due to the root-mean-square (rms) of the beam-waveguide mirrors, which is significant at Ka-band. Assuming an average 3-mil rms for each of the six mirrors, the loss of an additional 7.06 percent needs to be factored in. Assuming an average atmosphere factor of 1.09, the total correction applied to the PO computed values to compare them to the measured values is 0.85266. Convolving the calculated radiation patterns with Keihm's Ka-band maps for the various Moon phases, the comparison with the measured noise temperature is shown in Fig. 5.

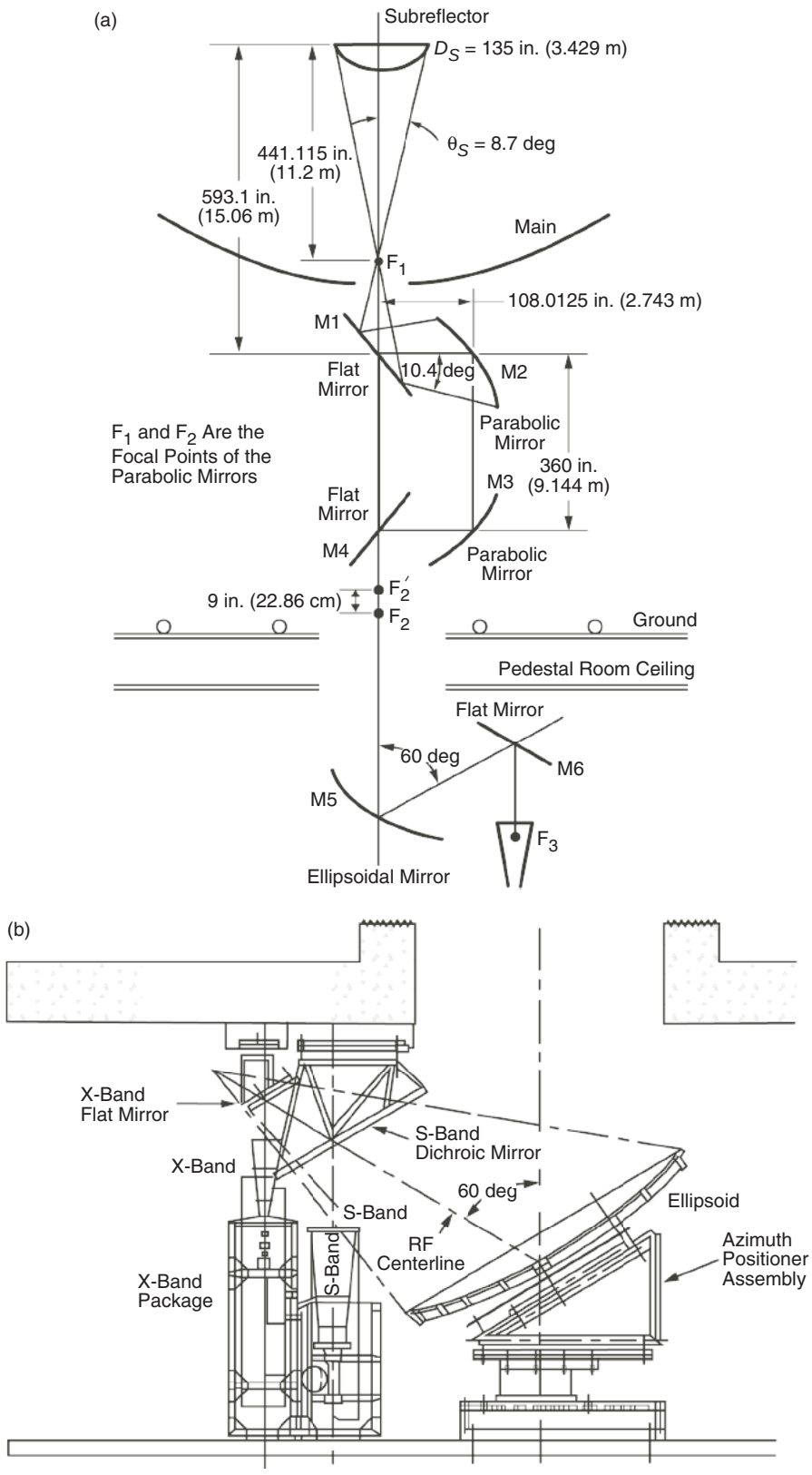

Fig. 1. DSS-13 BWG antenna S-/X-band position: (a) BWG mirrors and (b) S-/X-band feed arrangement.

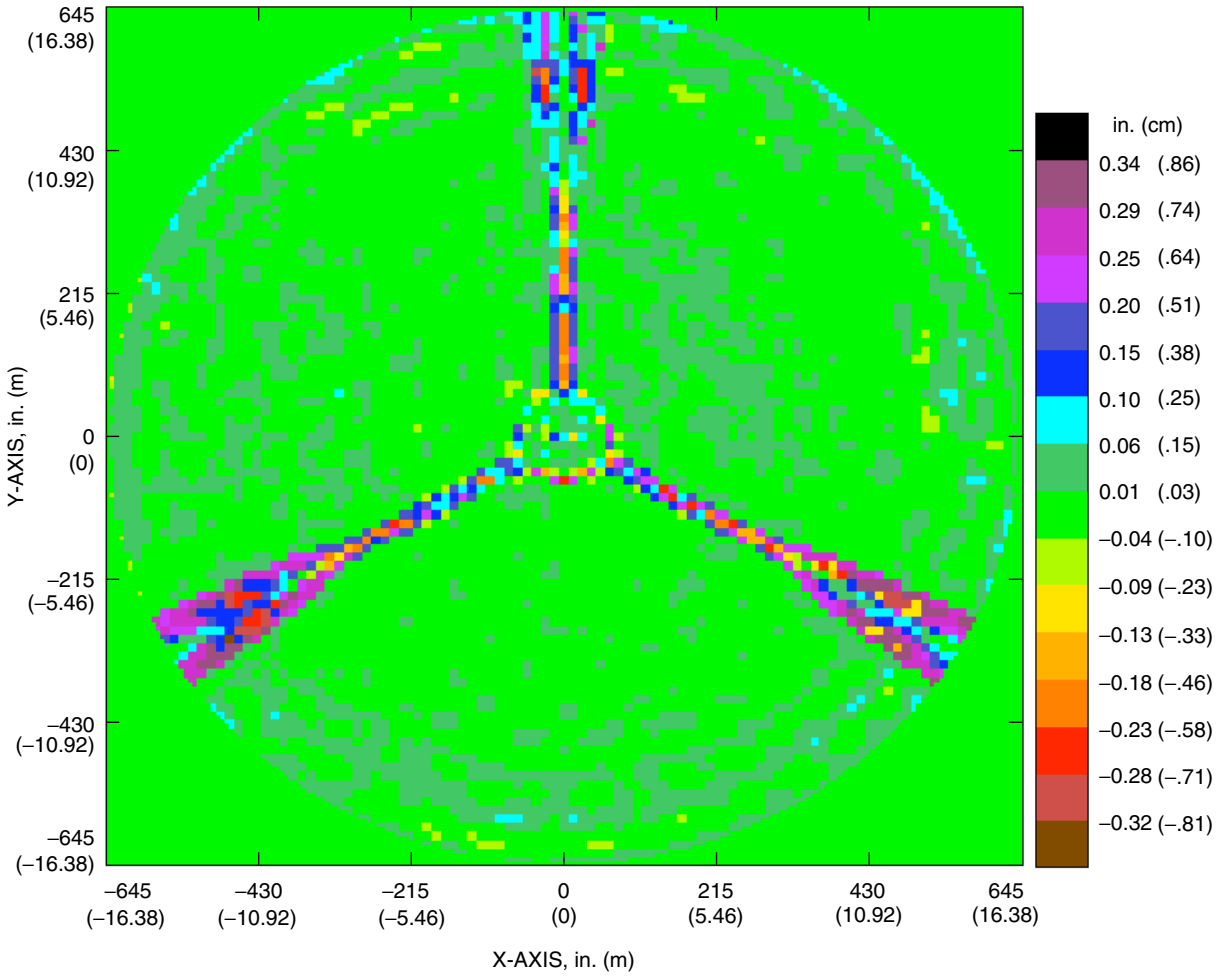

Fig. 2. Surface error at the rigging angle generated from holography data.

An interesting question that needs to be considered is the effect of surface distortion due to gravity as a function of elevation. Using the measured holography maps of the distortion, computations were made for noise-temperature differences for 5- to 85-deg elevation angles at the Moon phase angle of 180 deg. The computed noise temperatures are shown in Table 1. Also shown are the PO calculated peak gains (not all losses are included since these do not vary with elevation angle). Even though there is a significant variation in peak gain, the energy is just redistributed over the Moon, and it has minimal effect on the measured temperature difference.

VI. Conclusions

A methodology was shown for computing the noise-temperature increase for a large antenna pointed at the Moon. The article covered a range of frequencies and considered a range of cases, from the antenna beam width being comparable to the Moon's diameter to the beam width being a small fraction of the Moon's diameter. The data were compared to measured results, and the agreement was excellent.

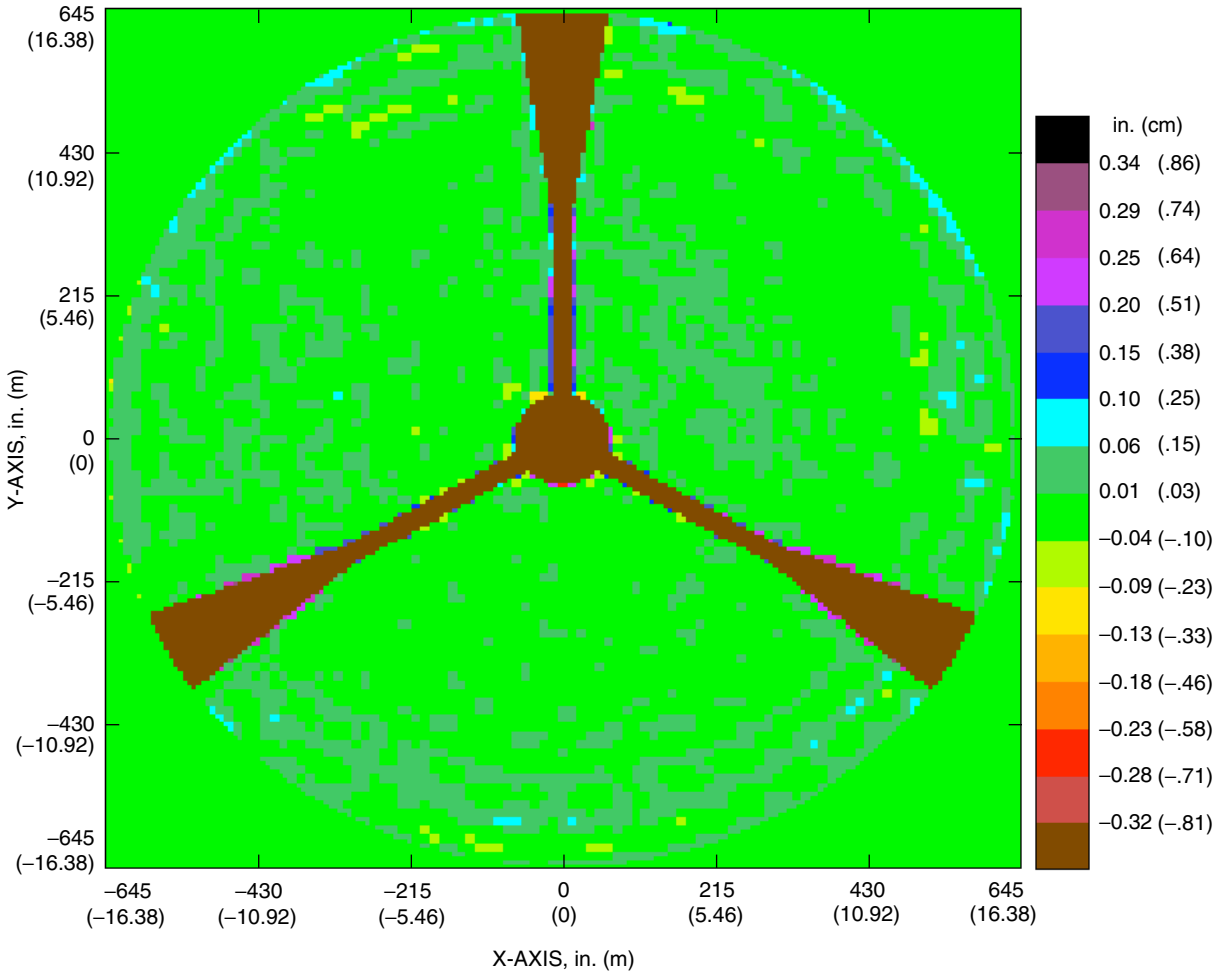

Fig. 3. Masking used for the struts and subreflector.

References

[1] D. D. Morabito, "Lunar Noise-Temperature Increase Measurements at S-Band, X-Band, and Ka-Band Using a 34-Meter-Diameter Beam-Waveguide Antenna," *The Interplanetary Network Progress Report*, vol. 42-166, Jet Propulsion Laboratory, Pasadena, California, pp. 1–18, August 15, 2006. http://ipnpr.jpl.nasa.gov/progress_report/42-166/166C.pdf

[2] W. A. Imbriale, *Large Antennas of the Deep Space Network*, Chapter 7, Hoboken, New Jersey: John Wiley and Sons, Inc., 2003.

[3] D. J. Rochblatt and B. L. Seidel, "Performance Improvement of DSS-13 34-Meter Beam-Waveguide Antenna Using the JPL Microwave Holography Methodology," *The Telecommunications and Data Acquisition Progress Report 42-108, October–December 1991*, Jet Propulsion Laboratory, Pasadena, California, pp. 253–270, February 15, 1992. http://ipnpr.jpl.nasa.gov/progress_report/42-108/108S.PDF

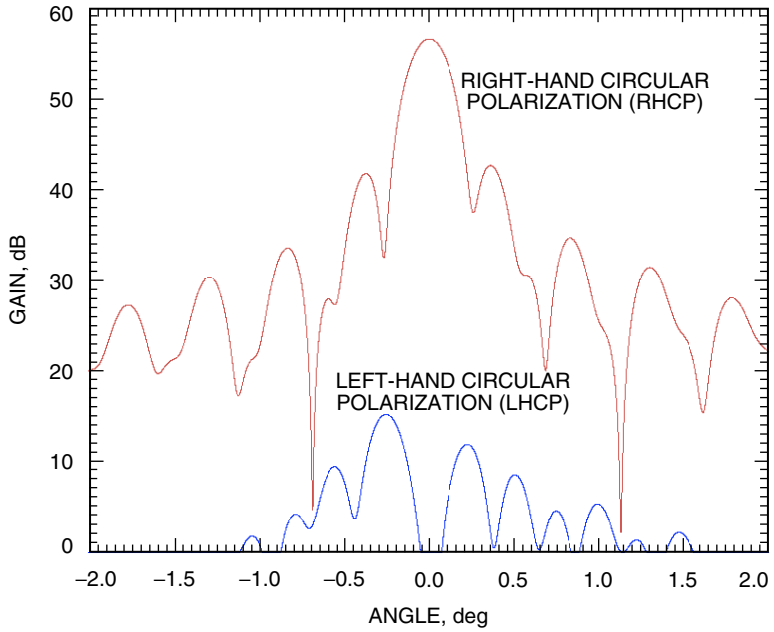

Fig. 4. Typical S-band radiation pattern.

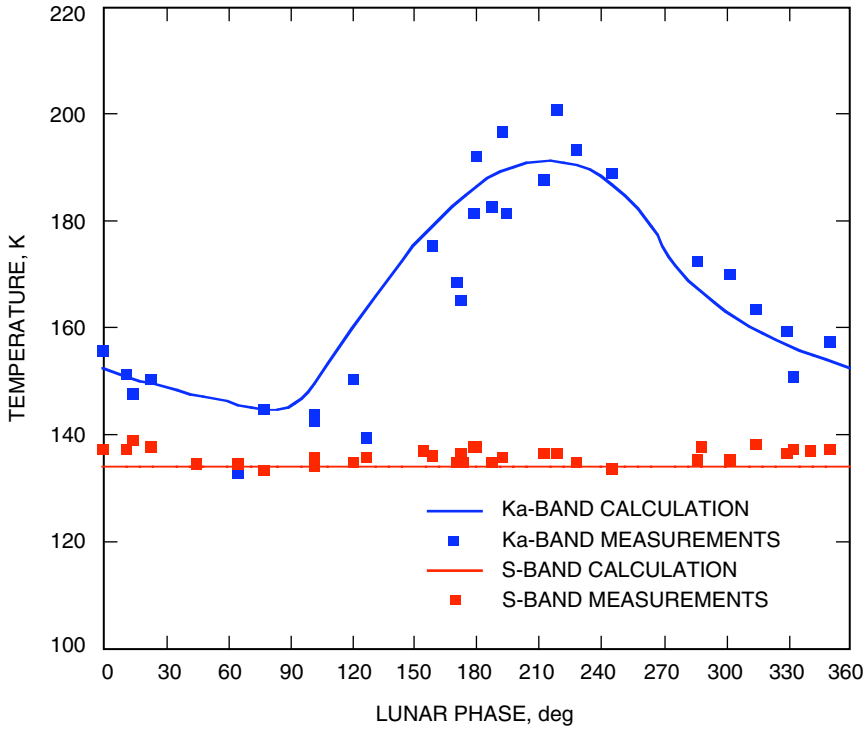

Fig. 5. Calculated and measured S-band and Ka-band difference temperatures.

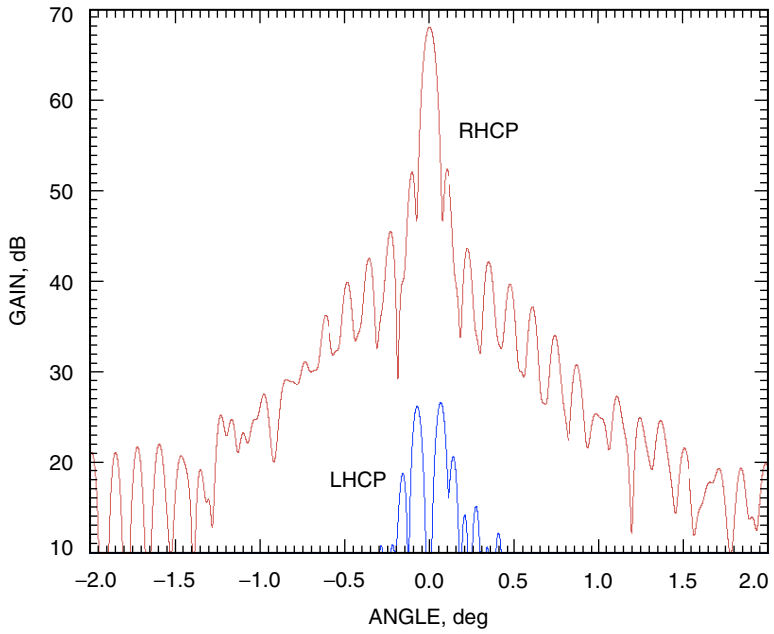

Fig. 6. Typical X-band radiation pattern.

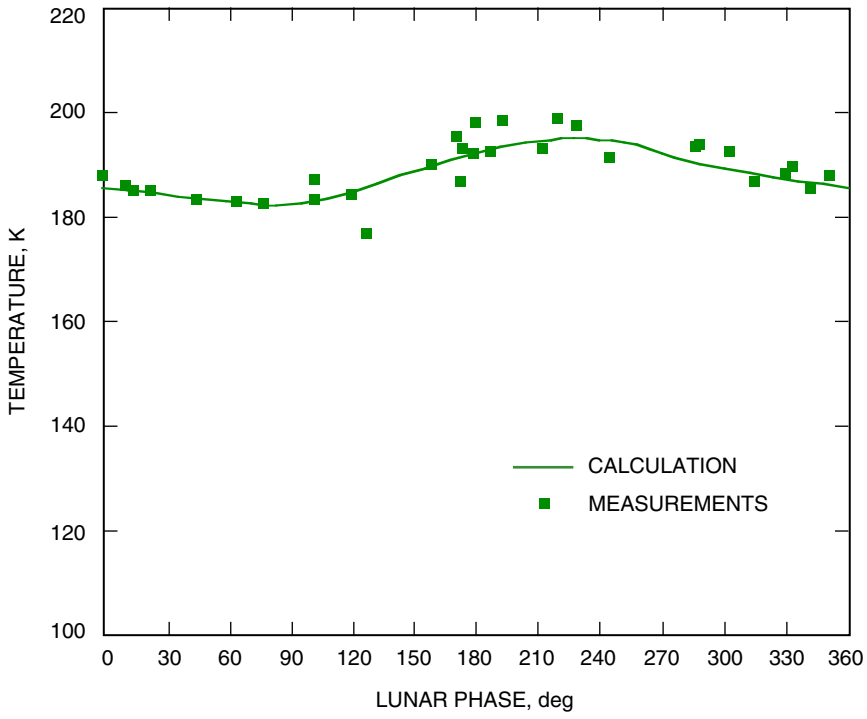

Fig. 7. Calculated and measured X-band difference temperatures.

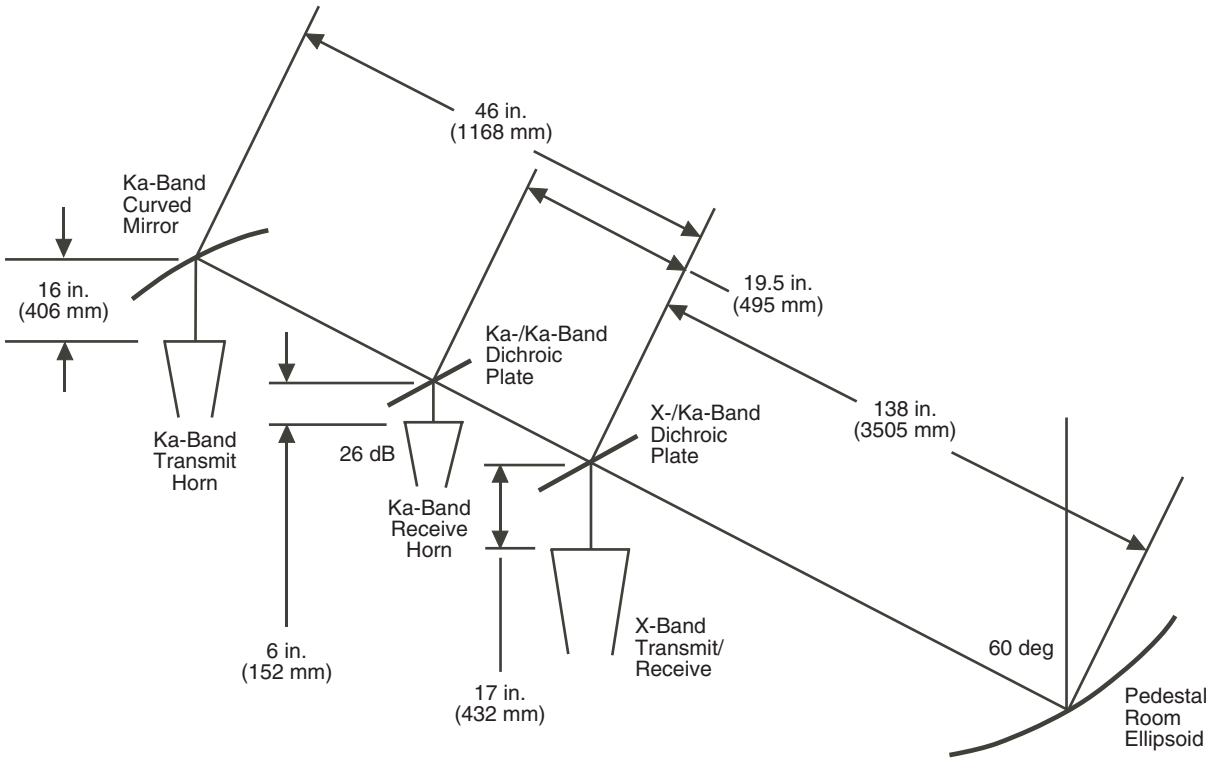

Fig. 8. DSS-13 X-/Ka-band position.

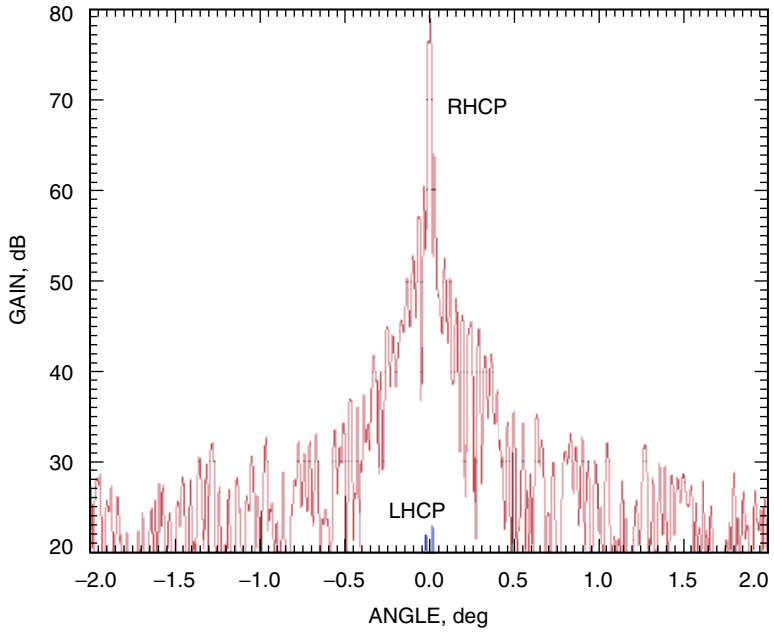

Fig. 9. Typical Ka-band radiation pattern.

Table 1. Ka-band on-axis gain and noise-temperature difference versus elevation.

Elevation angle, deg	PO calculated gain, dB	Difference temperature, K
5	76.10	184.6
15	77.61	188.0
25	78.13	176.8
35	78.62	176.3
45	79.14	186.1
55	78.81	178.8
65	78.28	174.4
75	77.87	181.6
85	76.71	184.3